RSC Advances

ROYAL SOCIETY
OF CHEMISTRY

www.rsc.org/advances

Enhancement of photoluminescence emission and anomalous photoconductivity properties of Fe_3O_4@SiO_2core-shell microsphere

[1]S. K. Jana*[†], [1]S. Majumder[†], [1]B. Satpati, [2]S. K. Mishra, [3]R. K. Srivastava, [1]S. Banerjee

[1]Surface Physics and Material Science Division, Saha Institute of Nuclear Physics
1/AF Bidhannagar, Saltlake, Kolkata - 700064, India

[2]Department of Physics, University of Lucknow, Lucknow- 226007, India

[3]Department of Electronics and Communication, University of Allahabad, Allahabad-211002, India.

Abstract

In this manuscript we report the successful synthesis of both pristine Fe_3O_4 and Fe_3O_4@SiO_2 core@shell structure. From SEM micrograph we observe that each Fe_3O_4 microsphere is composed of large number of smaller nanoballs. We have studied extensively photoluminescence and photoconductivity property of both pristine and SiO_2 coated Fe_3O_4 particle for the first time. Enhancement of photoluminescence emission is observed in Fe_3O_4@SiO_2 core@shell samples while reduced and negative photoconductivity is observed in the same sample. SiO_2 coating reduces the concentrations of non-radiative trap levels at the interfaces of core and shell thereby resulting in enhancement of photoluminescence intensity in core-shell particles. An exponential rise and decay in photocurrent is observed upon UV irradiation in ON & OFF state respectively for Fe_3O_4 whereas, for Fe_3O_4@SiO_2 we observe a transient rise in photocurrent and this photocurrent is not stable, we have explained this unusual behavior of photocurrent.

*E-mail: skj_ec@yahoo.co.in

1

(1) Introduction

Recently core/shell structured nanoparticles have received much attention due to their modified optical, electronic and magnetic properties compared to those of single-component nanomaterials [1]. Among all the currently studied nanomaterials, Fe_3O_4 is one of the most popular one and it has been found to have large applications in information storage, magnetic refrigeration, magneto optical solid devices, cell separation and magnetic resonance imaging enhancement [2-4]. Structural and magnetic property of SiO_2 coated Fe_3O_4 has been discussed elaborately in some earlier reports [5-7], where the SiO_2 coating not only provides a chemically inert surface for magnetic nanoparticles but also allow the nanoparticle to conjugate its surface with various functional groups. Since surface defect of nanostructured material is known to have a great influence on its optical property [8-10], studies of photo response of both Fe_3O_4 and $Fe_3O_4@SiO_2$ core-shell system has drawn much attention in the photonic research field. Photocatalytic property of Fe_3O_4 and $Fe_3O_4@SiO_2$ core-shell particles at high energy of incident spectrum [5-7] has been reported but investigations of PL and PC on such kind of samples have not been reported so far. In this manuscript we report the effect of SiO_2 shell on PL and PC.

Several groups have investigated the photoconductivity of silica based nanocomposite system [11-14]. Enhanced photoconductivity has also been observed on SiO_2 based ZnO nanocomposites [11-13] and reduced photoconductivity was reported on ZnO quantum dot embedded in SiO_2 matrix [14]. The PC study depends exclusively on the surface properties of the nanomaterials. Various explanations have been proposed to explain the PC of different oxide materials [15-17]. Broadly, two different mechanisms have been proposed for the origin of PC; first is the fast band to band transition with characteristic time in nanosecond range and second is the adsorption/desorption of oxygen molecules at the interfaces of nanomaterials (where the holes generated upon illumination helps in discharging oxygen species from the surfaces by indirect electron hole recombination mechanisms [14]).

In this paper, we have studied for the first time the unusual optical property of Fe_3O_4 based core-shell particle. Both pristine Fe_3O_4 and $Fe_3O_4@SiO_2$ core-shell structures have been successfully synthesized. It is investigated that how the surface morphology of Fe_3O_4 affects its PL and PC property. Also we have discussed in detail the influence of SiO_2 coating i.e., the surface property, on the PL and PC of the $Fe_3O_4@SiO_2$ core-shell particles.

2

(2) Experimental

Core-shell microsphere sample was synthesized by two steps method; (i) synthesis of Fe_3O_4 microspheres (core formation) followed by (ii) coating of it with SiO_2 (shell formation). 2.7gm of iron chloride (III) hexahydrate, 2.0 gm of polyethylene glycol (PEG, M_w = 4000) and 7.2 gm of sodium acetate trihydrate were added into 80 mL ethylene glycol under constant magnetic stirring. Then the solution was transferred into a teflon lined stainless steel autoclave with capacity of 100mL, and heated at 180°C for 19h. The product was collected, washed with de-ionized (DI) water and absolute ethanol and finally dried at 65°C for 3h. For the preparation of SiO_2 coated particles, 0.4g of as-prepared Fe_3O_4 was dispersed into a mixture of 40mL ethanol and 8mL DI water in a glass beaker under constant stirring. Then 2mL of ammonia solution (25 wt %) and 1.6mL of tetraethyl orthosilicate (TEOS) were consecutively added and kept under constant stirring for 3h. Finally, the resultant products were collected, washed and dried at 65°C for 3-6 h.

Structural analysis of both pristine and $Fe_3O_4@SiO_2$ core-shell was carried out by X-ray diffractometer (Bruker AXS D8) using Cu Kα radiation. The surface morphology of both pristine Fe_3O_4 and $Fe_3O_4@SiO_2$ core-shell was obtained from scanning electron microscopy (SEM) measurement and detailed structural information was carried out using transmission electron microscopy (TEM: FEI, TF30, ST microscope operating at 300 kV) investigations. The TEM is equipped with a scanning unit and a high angle annular dark-field (HAADF) detector from Fischione (model: 3000). The samples were mounted on a carbon coated Cu grid, and used for TEM measurements.

Room temperature photoluminescence (PL) measurements were performed on both samples with same concentration of aqueous solution using JASCO spectroflurometer (FP 6700) at an excitation of 320nm keeping the fixed slit width of 2.5nm in both cases.

The photo and dark conductivities of both pristine and SiO_2 coated Fe_3O_4 NPs were measured using thick film of samples in between interdigitated Cu electrodes. The two electrodes top with thick sample was pressed with a transparent glass plate. This glass plate had a slit for providing illumination area of 0.25 cm^2. In this cell type device, the direction of illumination was normal to field across the electrodes. The cell was mounted in a dark chamber with a slit where

from the light was allowed to fall over the cell. The photoresponse was measured with 300 W mercury lamp under UV illumination of 365 nm of fixed intensity as an excitation source. A stabilized dc field (5 V/cm to 50 V/cm) was applied across the cell and both dark current & photocurrent were measured by a nanoampmeter (NM122, Scientific Equipment) in series with a RISH 15S multimeter connected with adapter RISH Multi SI 232. Before measuring photoconductivity of the sample, the cell was first kept in dark till it attains equilibrium.

(3) Results and discussions

Structure and morphology of pristine Fe_3O_4 and $Fe_3O_4@SiO_2$ were analyzed using both SEM and TEM images shown in of Fig. 1 and 2 respectively. From the Fig. 1a, it is observed that Fe_3O_4 microspere is formed of large number of Fe_3O_4 nanoballs and Fig. 1b reveals the core-shell formation of $Fe_3O_4@SiO_2$ where Fe_3O_4 microsphere appears as core and a thin layer of SiO_2 as shell. Also it is confirmed that large number of PEG capped Fe_3O_4 nanoparticles agglomerate to form a Fe_3O_4 microsphere as shown in Fig. 1c.
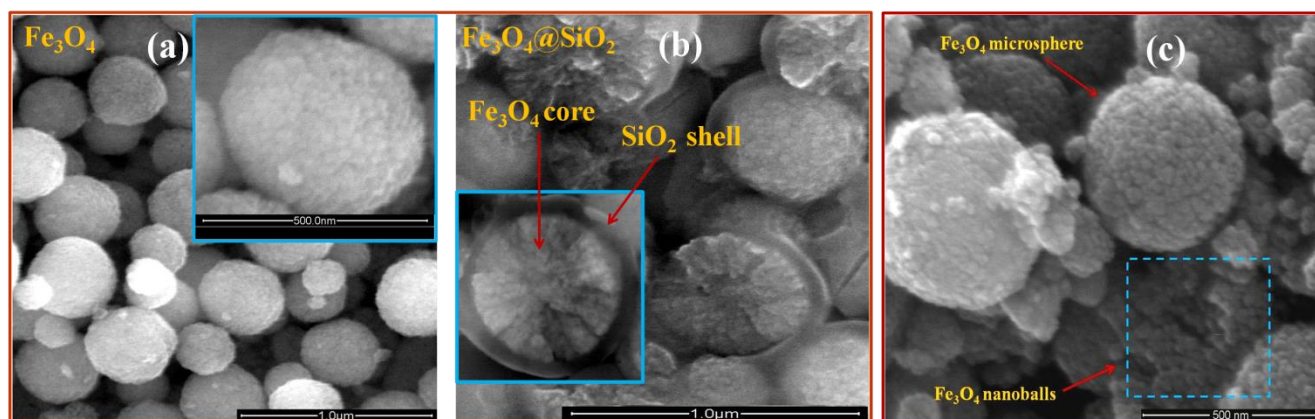
Fig. 1: SEM morphology of (a) Fe_3O_4 (b) $Fe_3O_4@SiO_2$ (c) formation of Fe_3O_4 microsphere from large number of Fe_3O_4 nanoballs.
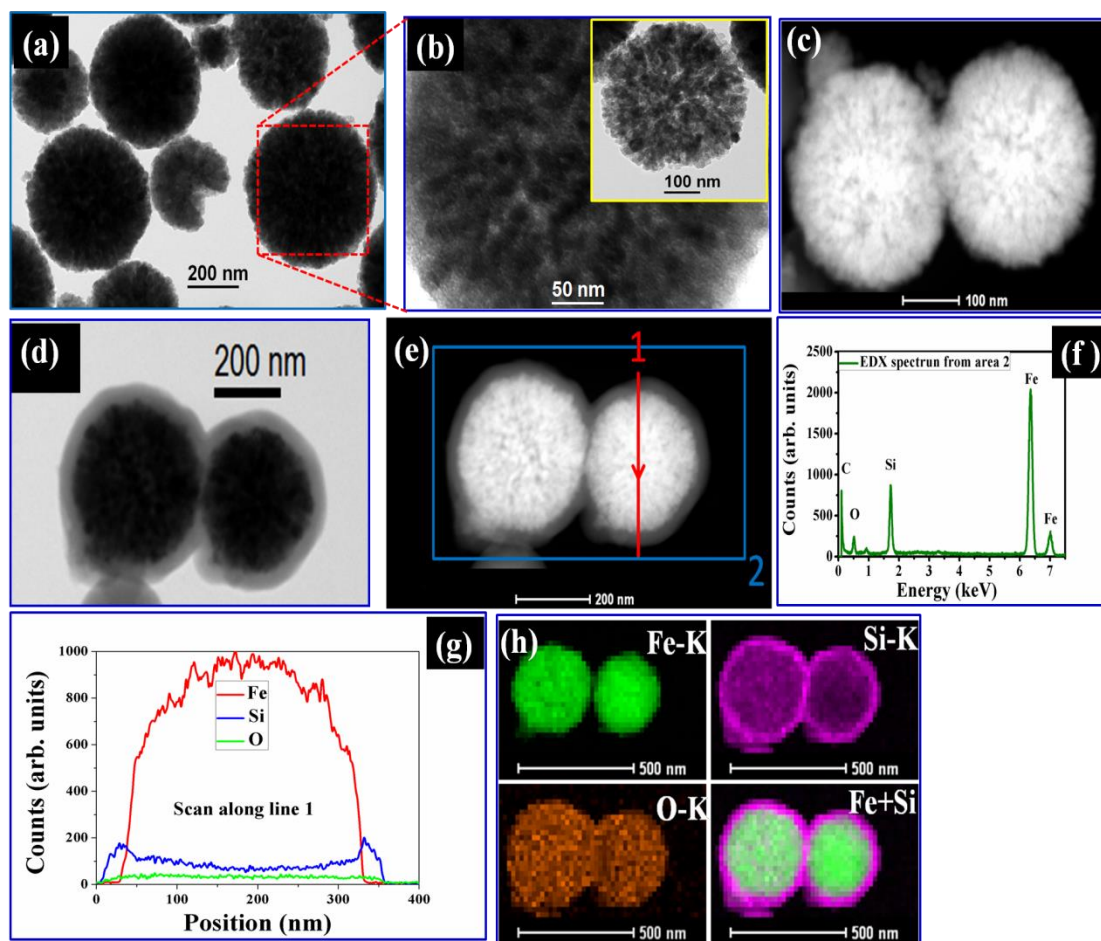
Fig. 2: (a)-(b) TEM images and (c) STEM-HAADF image of Fe_3O_4 microsphere. (d) TEM image and (e) STEM-HAADF image of $Fe_3O_4@SiO_2$ microsphere. (f) Selected area ('2') EDX analysis and (g) line scan EDX analysis of $Fe_3O_4@SiO_2$. (h) Elemental color mapping of $Fe_3O_4@SiO_2$ cores-shell sample.

Fig. 2a shows the TEM image of pristine Fe_3O_4 microspheres which are consistent with the SEM image of pristine sample. Also high resolution TEM image (shown in Fig. 2b) confirms that the Fe_3O_4 microspheres are consisting of smaller Fe_3O_4 nanoparticles. We observe that arrangement of Fe_3O_4 nanoparticles inside microsphere creates some voids spaces which can be seen in the inset of Fig 2b. High angle annular dark-field scanning transmission electron microscopy (STEM-HAADF) image (shown in Fig. 2c) of Fe_3O_4 is consistent with SEM image of the same sample shown in Fig. 1a. Both TEM image and STEM-HAADF image of Fig. 2d & 2e demonstrate the successful synthesis process of the core-shell particles. Energy dispersive X-

ray (EDX) spectrum in Fig. 2f from area 2 in the STEM-HAADF image (Fig. 2e) and subsequent line scan along line 1 and elemental map from area 2 (Fig 2g and Fig. 2h respectively) confirmed that the core material is Fe_3O_4 and SiO_2 is formed as shell.
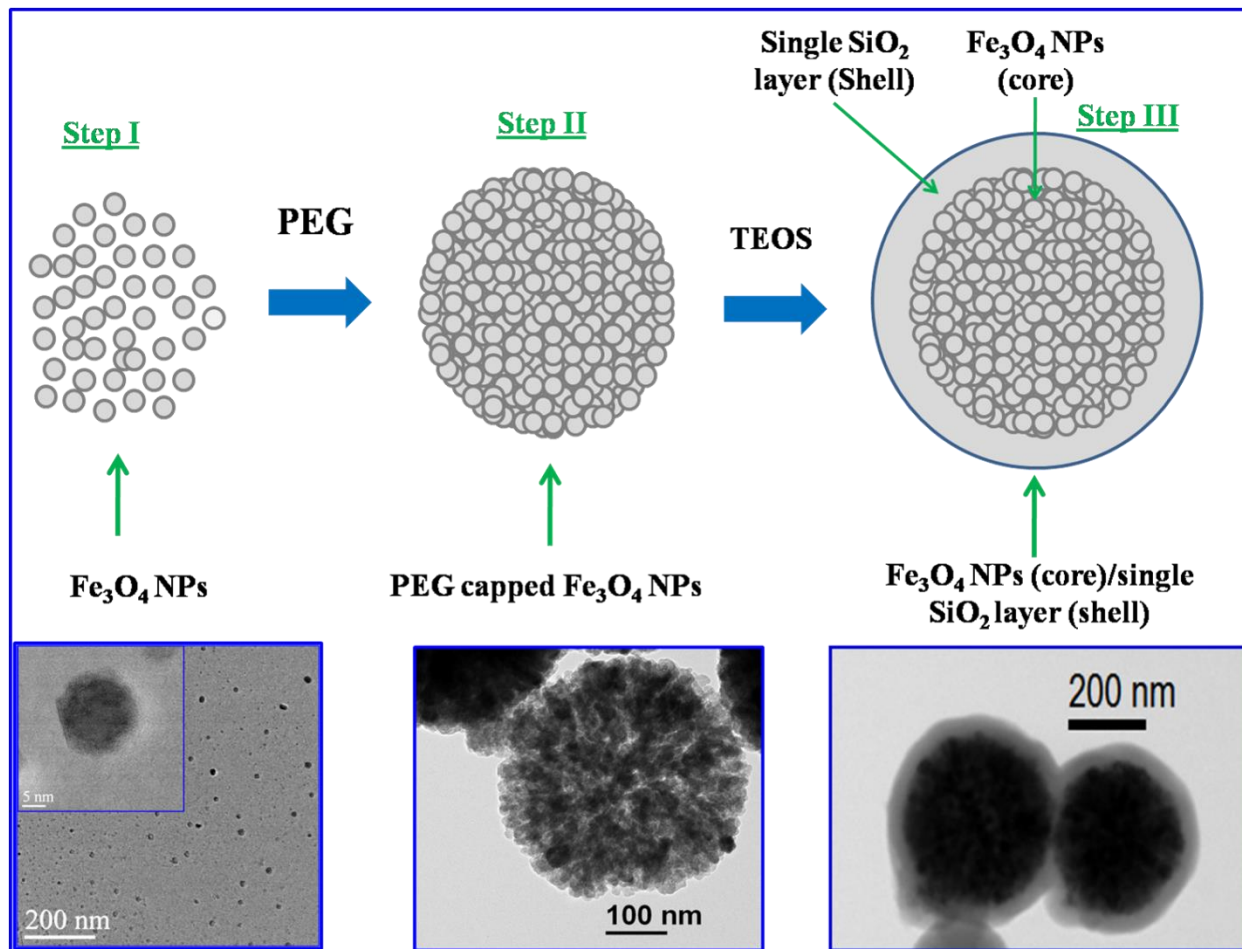
Fig. 3: Schematic representation of formation of both Fe_3O_4 and $Fe_3O_4@SiO_2$.

The formation mechanism of bare and SiO_2 coated Fe_3O_4 (core/shell) microsphere is shown schematically in Fig. 3. TEM images are also shown individually bellow of each formation mechanism step of the schematic. In the first step we have synthesized PEG capped Fe_3O_4 NPs of sizes ~ 18nm (first TEM image of schematic) through co-precipitation method. Also HRTEM image of the individual Fe_3O_4 NPs shows lattice fringes which prove the NPs are crystalline in nature. In the second step, there is a large number of Fe_3O_4 NPs agglomerate to form Fe_3O_4 microsphere as shown in second TEM image of the schematic. In the last step, a thin

layer of SiO_2 cell has been formed on Fe_3O_4 microsphere by hydrolysis of TEOS followed by a cross linking with Fe_3O_4 as shown in the schematic diagram and we obtained $Fe_3O_4@SiO_2$ core-shell particle shown in the TEM image. The mechanism behind the formation of Fe_3O_4 microsphere is magnetite nanocrystals nucleate first in a supersaturated solution which is the solvent-mediated hydrolysis of Fe^{3+}. Afterward, the newly formed nanocrystals aggregate into round spheres, driven by minimization of total surface energy [18].
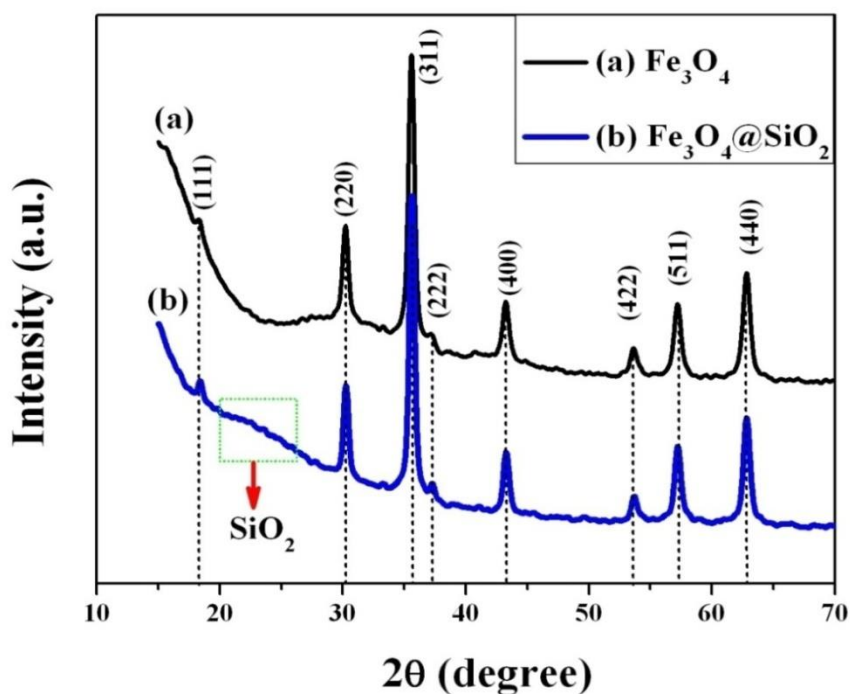
Fig. 4: XRD pattern of (a) Fe_3O_4 (b) $Fe_3O_4@SiO_2$.

Crystallographic phases of both Fe_3O_4 and $Fe_3O_4@SiO_2$ sample was identified by X-ray diffraction analysis as shown in Fig. 4. The diffraction peaks at 30.2, 35.6, 39.5, 43.1, 46, 53.7, 57.1 and 62.7^0 corresponds to [220], [311], [400], [511], and [440] planes of Fe_3O_4 which are consistent with earlier report [19-20]. The positions of all the diffraction peaks of Fe_3O_4 powder are well matched with the standard JCPDS 19-629. The diffraction pattern indicates that the Fe_3O_4 particles are single phase and belong to the cubic system. For $Fe_3O_4@SiO_2$, the small hump from $20.5°$ to $25°$ is due to the amorphous SiO_2 shell which is also consistent with earlier reports [20]. Hence, it can be concluded that the SiO_2 coating on Fe_3O_4 has not changed the

crystal structure of the core Fe_3O_4 particle. The successful conjugation of SiO_2 onto the surface of the Fe_3O_4 was confirmed by Fourier transform infrared (FTIR) measurements. The FTIR spectra of (a) Fe_3O_4, (b) $Fe_3O_4@SiO_2$ are shown in Fig. 5. In Fig. 5a, the band at 567 cm^{-1} is related to the Fe-O bending vibration while the band at 574 cm^{-1} in Fig. 5b is an indication of the presence of Si-O-Fe stretching vibration [21].
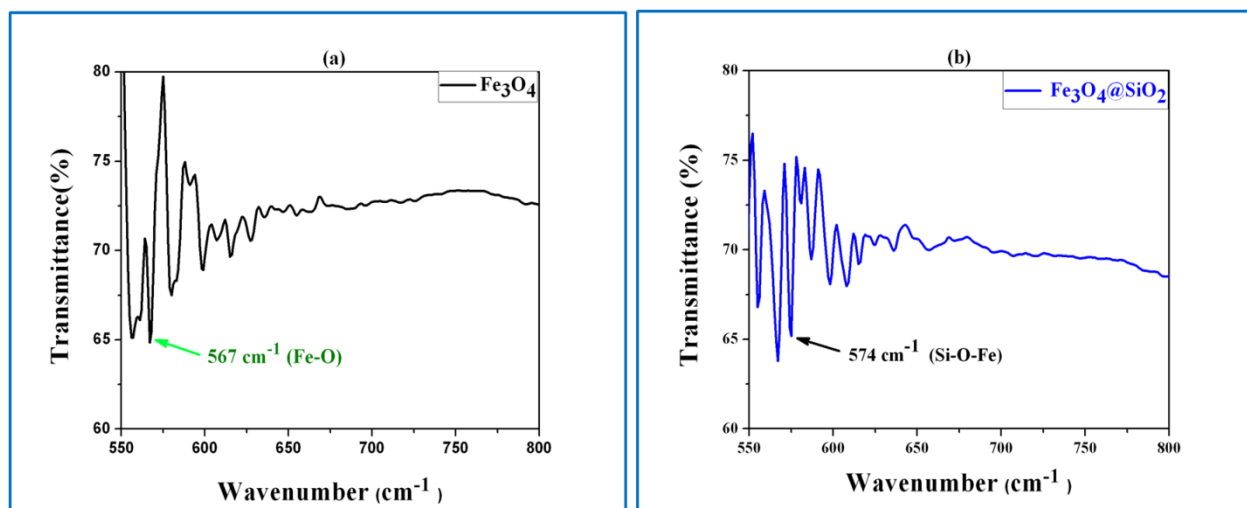
Fig. 5: FTIR spectra of (a) Fe_3O_4 (b) $Fe_3O_4@SiO_2$.
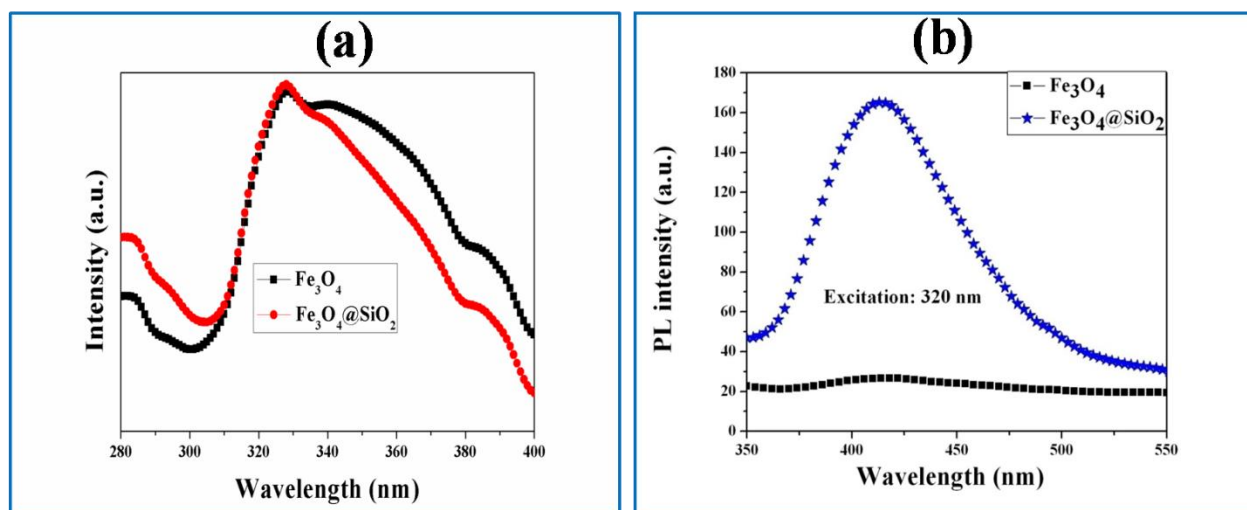
Fig. 6: (a) PLE measurements of both Fe_3O_4 (black line) and $Fe_3O_4@SiO_2$ (blue line) samples (b) Room temperature PL measurements of both Fe_3O_4 (black line) and $Fe_3O_4@SiO_2$ (blue line) samples at an excitation wavelength of 320 nm.

Photoluminescence excitation (PLE) measurements were done keeping emission wavelength fixed at 450 nm. PLE curves of both the samples are shown in Fig. 6a. From this figure, it is observed that both the samples show a pronounced absorption peak between 305-400 nm which is consistent with the earlier report [22] on the absorption property of same samples. The peak position (~327 nm) of the PLE spectra attributes to the band edge excitation of both the samples. Also there is no peak shift of PLE spectra for the core-shell structure. So we can say that there is no change in bandgap of the core-shell particle. But the PLE spectra of $Fe_3O_4@SiO_2$ core-shell particles having much sharper absorption edge (after 327 nm) compared to the pristine Fe_3O_4 gives some indication of the modified surface properties of pristine Fe_3O_4 after SiO_2 coating.

PL emission peak of both pristine Fe_3O_4 and $Fe_3O_4@SiO_2$ at an excitation wavelength of 320 nm is shown in Fig. 6b and it can be seen that the emission wavelength at 414 nm is the same for both the two samples. The broad emission peak in Fe_3O_4 is observed because of oxygen vacancies which play a key role for the origin of violet emission similar to the green PL observed in ZnO. [8-10]. Fe_3O_4 nanoparticles have very large surface area and so have large number of dangling bonds associated with oxygen vacancy which constitutes the surface defects. This defects form a donor states below the conduction band. The PL emission arises from the recombination of electrons in the donor states with photoexcited holes in the valence band. Furthermore, Fe_3O_4 sphere shows broadening of the PL emission with reduced intensity which is the result of scattering of the incident and emitted photons from the highly roughened surface of Fe_3O_4. SEM and TEM images show that the Fe_3O_4 spheres have the surface voids and surface roughness which are mostly caused by the Fe_3O_4 small particles agglomeration. Upon SiO_2 coating, the density of the surface dangling bonds are reduced due to the formation of Fe-O-Si on core-shell structure as shown in FTIR spectrum of Fig. 5. Hence, the SiO_2 coating reduces the number of trap states and surface states. Thus the probability of blue-green emission through radiative recombination is increased due to the reduction in the concentrations of non-radiative trap levels [11, 23]. Thus we observe that coating of SiO_2 on Fe_3O_4 enhances the PL property of Fe_3O_4. Moreover, the outer SiO_2 layer decreases the surface voids and as well as the roughness also. Therefore enhanced and coherent emission from the core-shell particle was obtained due to reduced light scattering by the SiO_2 coating.
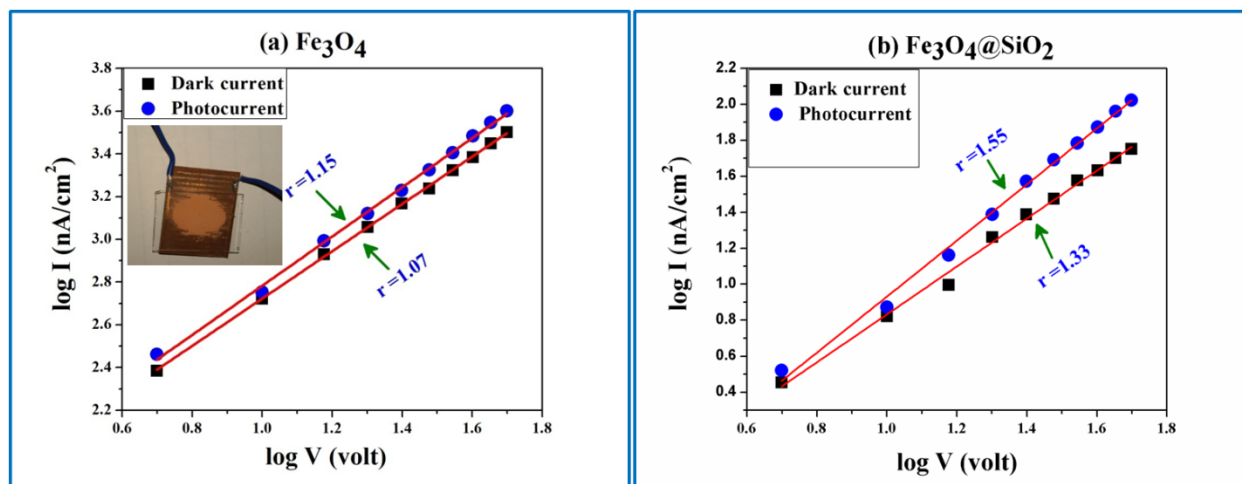
9

Fig. 7: Figure 6: I-V characteristics of (a) pristine Fe_3O_4 (inset image shows the device structure for the photocurrent measurement of the samples) (b) $Fe_3O_4@SiO_2$.

Fig. 7a and 7b show the I–V characteristics of the samples. The variation of dark current (I_{dc}) and photocurrent (I_{pc}) with applied cell voltage on a log–log scale in dark and under UV light illumination ($\lambda = 365$ nm) is shown for both pristine and core-shell Fe_3O_4 microsphere, respectively. These two graphs clearly represent the linear variation with different slopes and can be expressed by the power law *i.e.* $I \propto V^r$, where I is either I_{pc} or I_{dc}, V is the applied DC voltage and exponent 'r' is the slope of straight line segment of the log-log plot. For pristine Fe_3O_4 sample, the variation of I_{dc} and I_{pc} with applied voltage is found to be non-Ohmic super linear [24-26] in nature for the entire voltage regime *i.e.* the power index is $1 < r < 2$. The non-Ohmic super-linear variation ($1 < r < 2$) in the dark current and photocurrent suggests that the charge carriers are being injected into the bulk of the materials produced from one of the electrodes [24]. This photoresponse confirms the feature of the sample itself, but not the feature of the sample-contact region. The value of 'r' is different for the two samples and the highest value of 'r' revealed by $Fe_3O_4@SiO_2$ may be attributed to the trapping of some of the photoexcited electrons in the SiO_2. From the I-V curves of both pristine and core-shell sample, it is obvious that the photocurrent for both the samples increases with voltage. It is clearly observed from Fig. 8 that the dark current in $Fe_3O_4@SiO_2$ sample is around ten times lower as compared to that in bare Fe_3O_4 sample. Similar trend is also found in the case of the photocurrent. In the composite

10

sample, the insulating layer of SiO_2 on Fe_3O_4 microspheres is the reason for the decrease in the dark current as well as the photocurrent.
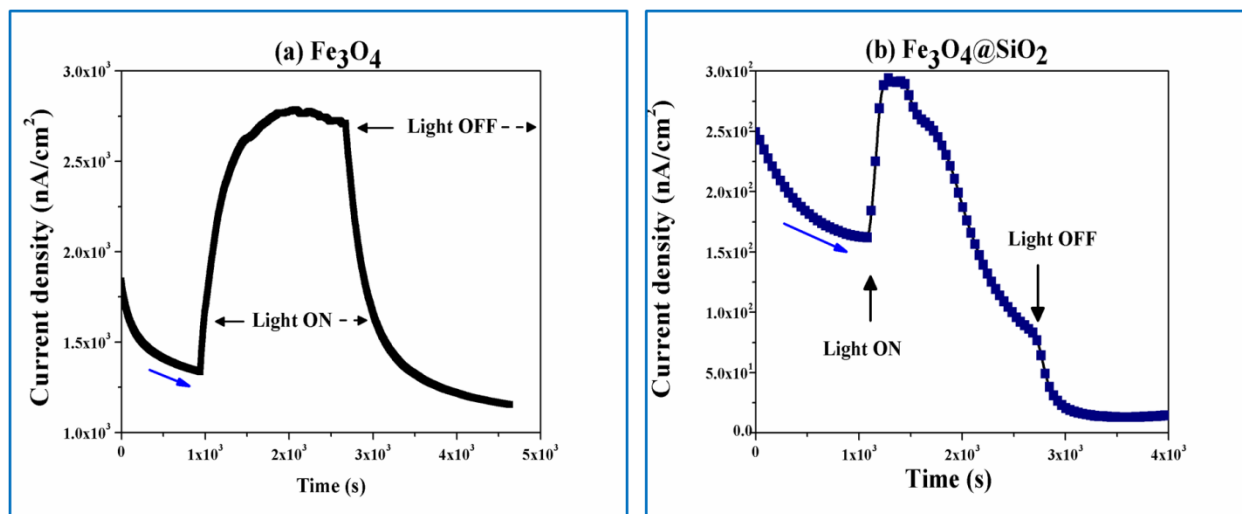
Fig. 8: Photocurrent rise-decay of (a) pristine Fe_3O_4 and (b) $Fe_3O_4@SiO_2$ core-shell samples respectively.

To further investigate the role of surface states/defects during UV On/Off conditions, time resolved rise and decay of photocurrent has been measured for both the samples keeping the biasing voltage fixed at 10V. The transient photocurrent response under steady state illumination of both samples is shown in Fig. 8a and 8b respectively. Before transient measurements the samples were kept in the dark till the current reached the equilibrium value. For the pristine Fe_3O_4 sample, when UV light is switched on, the photocurrent raises upto 90% of its peak value within ~400 s then it attains its peak value and gets saturated. When the light is switched off, the photocurrent decays upto 90% within 95s. In case of the composite sample, when the UV light is illuminated the photocurrent rises upto 90% of its peak value within 105s. After attaining a peak value, it starts decaying slowly even during steady illumination and eventually reaches a value lower than the value of the dark-current which may be attributed to the carrier relaxation at the SiO_2 coating. This observation is similar to the negative photoconductivity observed by S. Panigrahi et. al in ZnO particle embedded in SiO_2 matrix [14]. This negative photoconductivity may be a common phenomenon in composite of SiO_2 and transition metal oxide systems. The detailed mechanism of transient response of both samples under dark and UV illumination is discussed elaborately below.

11

It is evident from Fig. 8a and 8b, initially the field dependent dark current starts decreasing slowly until it achieves the steady value (marked by blue arrow in both Fig. 8a and 8b) which may be attributed to the field induced adsorption of oxygen molecule as well as due to presence of defects [27]. In the absence of UV light, oxygen is adsorbed by taking a free electron from the surface of Fe_3O_4 nanoballs. The adsorbed oxygen molecules (O_2) on the surface of both pristine Fe_3O_4 and $Fe_3O_4@SiO_2$ core-shell particles become negatively charged ions $[O_2 + e^- \rightarrow O_2^-(ad)]$ after capturing the free electrons from both Fe_3O_4 and $Fe_3O_4@SiO_2$ core-shell particles and develop a depletion layer near the film surface of low conductivity.

Thus surface of both type of particles are almost depleted of carriers leading to low conductivity in dark [28-30]. Under UV illumination, the photogenerated electron - holes are produced and the captured species (O_2^- ion) are released by the process $O_2^-(ad) + h^+ \rightarrow O_2$ (g). The adsorbed oxygen molecules are released in air, which lowers the barrier height for the electrons in Fe_3O_4 sample. This mechanism was proposed by Muraoka et al. in Ref. [31]. When all photoinduced holes react with O_2^-, photo current gets saturated in Fe_3O_4 samples. Also it is seen that the photocurrent of $Fe_3O_4@SiO_2$ is reduced significantly compared to pristine Fe_3O_4 microsphere. Decrease of photoconductivity has been observed in ZnO quantum dot embedded in SiO_2 matrix [14], Si nanocrystals in SiO_2 [32], CdSe embedded in SiO_2 [33]. In $Fe_3O_4@SiO_2$ core-shell structure, the surface properties of Fe_3O_4 microsphere are quite different because of the formation of long chain SiO_2 network around Fe_3O_4 core particle. The lower photocurrent observed in the case of $Fe_3O_4@SiO_2$ sample is explained with the help of a schematic diagram shown in Fig. 9 below.

The lower photocurrent observed in $Fe_3O_4@SiO_2$ sample as compared to that in pristine Fe_3O_4 sample could be explained on the basis of adsorption/desorption processes on the surface of the samples. The concentration of adsorbed oxygen molecules on Fe_3O_4 surface depends upon the concentration of dangling bonds on the surface of the sample and as surface to volume ratio in nano Fe_3O_4 is large, the surface phenomena of adsorption/desorption plays a significant role. Oxygen molecules get adsorbed on the surface of Fe_3O_4 and when the surface is illuminated by UV-vis light, photogenerated holes release the adsorbed oxygen from the surface of Fe_3O_4 and the photoinduced electrons gives rise to the photocurrent in pristine Fe_3O_4 sample. In case of $Fe_3O_4@SiO_2$ core-shell sample, a significant proportion of the surface of Fe_3O_4 nanoparticles are

passivated with SiO_2 layer (passivation of such Fe_3O_4 nanoparticles is shown by black lines in Fig. 9) that results in reduction of adsorption sites for O_2 molecules.
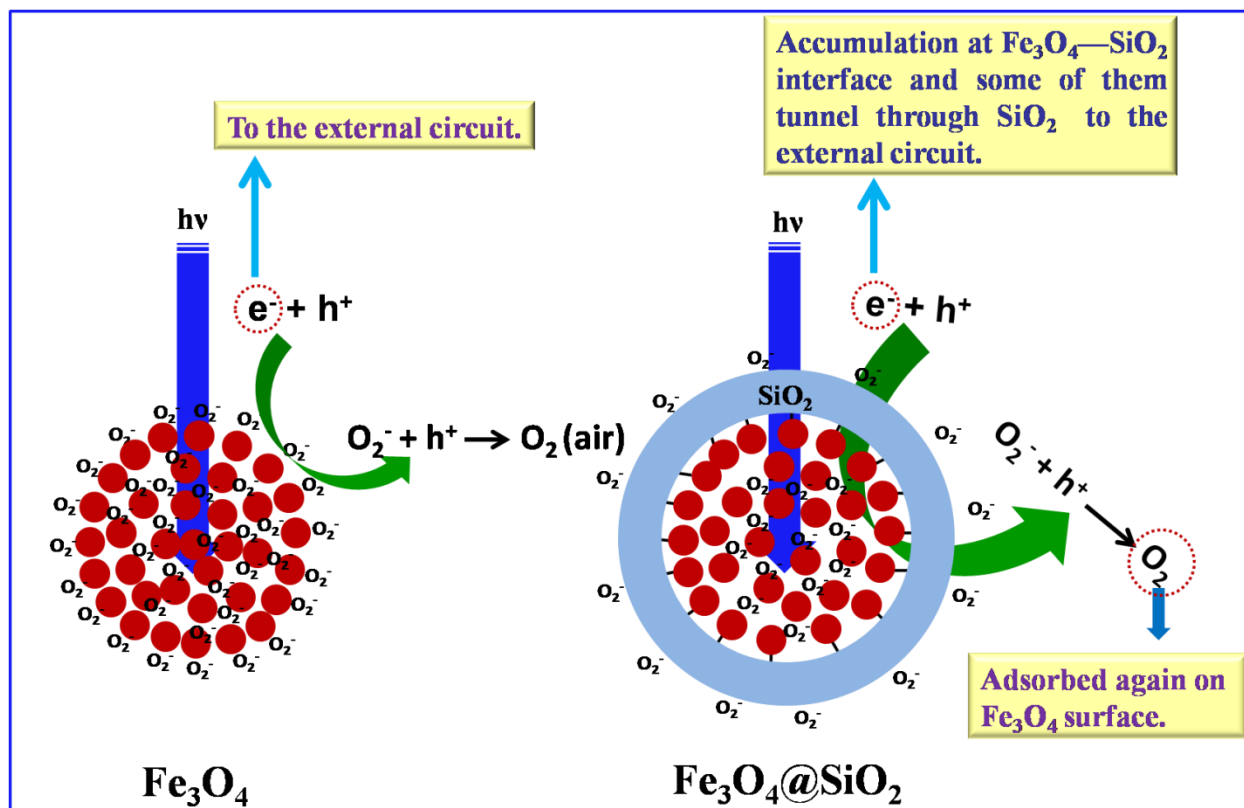
Fig. 9: Schematic representation of the mechanism of anomalous photoconductivity exhibited by Fe_3O_4@SiO_2.

Photocurrent in core shell may be attributed to desorption of O_2 molecules from the surface of SiO_2 layer as well as from the surfaces of non-passivated Fe_3O_4 nanoparticles. As the SiO_2 layer is having thickness in the range of 25-30 nm which is lower than skin depth for SiO_2 in UV region, a small portion of UV illumination (high energy photons) penetrates the shell and reaches the core to interact with the non-passivated Fe_3O_4 nanoparticles and since the surface to volume ratio gets reduced in the core-shell structure as compared to that in pristine Fe_3O_4 nanopartcles, photocurrent as a result of desorption of O_2 molecules in core-shell nanostructure gets reduced as compared to that in pristine Fe_3O_4 nanoparticles. A few electrons tunneling through the SiO_2 layer help O_2 to get adsorbed on the Fe_3O_4 surface under dark condition, while upon UV illumination photogenerated holes release O_2 molecules which cannot come out from core into the ambient. As a result the electrons are accumulated at Fe_3O_4-SiO_2 interface. Anomalous

behavior of photocurrent in core-shell nanostructure may be attributed to this re-adsorption of the desorbed O_2 molecules on the surface of non-passivated Fe_3O_4 nanoparticles after getting accumulated electrons from the Fe_3O_4-SiO_2 interface. Therefore, because of the adsorption and desorption mechanism of oxygen occurring simultaneously under continuous illumination, we observe anomalous drop in the photocurrent giving rise to the negative PC. After the UV is OFF the decay current follows the oxygen adsorption mechanism [34-35]. Thus, when the illumination is terminated, the current reduces faster due to fast recombination of electron and holes.

(4) Conclusions

In summary, we could encapsulate Fe_3O_4 microsphere made of nanoparticles with SiO_2 shell successfully. We observed enhanced PL and negative PC in Fe_3O_4@SiO_2 core@shell but Fe_3O_4. micorspheres exhibited reduced PL intensity and enhanced PC. The enhanced PL emission in Fe_3O_4@SiO_2 samples is attributed to the reduction the non radiative trap levels at the interfaces of smaller nanoballs after SiO_2 coating. Since SiO_2 shell formation reduces the oxygen adsorption sites and the tunneling of electrons among the particles leads to anomalous behavior of negative photoconductivity in Fe_3O_4@SiO_2. To conclude, pristine Fe_3O_4 can be utilized for UV photodetection and optical switches while Fe_3O_4@SiO_2 core@shell samples might be used for luminescent material due to enhanced PL intensity.

Author contributions

†These authors contributed equally to this work.

References

[1] Q. H. Lu, K. L. Yao, D. Xi, Z. I. Liu, X. P. Luo, Q. Ning, Nanoscience. 11 (2006) 241-248.

[2] G. H. Du, Z. L. Liu, X. Xia, Q. Chu, S.M. Zhang, J. Sol-Gel. Sci. Techn. 39 (2006) 285–291.

[3] S. Banerjee, S. O. Raja, M. Sardar, N. Gayathri, B. Ghosh, A. Dasgupta, J. Appl. Phys. 109 (2011) 123902-123907.

[4] Z. L. Liu, Y. J. Liu, K. L. Yao, Z. H. Ding, J. Tao, X. Wang, Journal of Materials Synthesis and Processing. 10 (2002) 83-87.

[5] E. Girgis, M. M. Wahsh, A. G. Othman, L. Bandhu and K.V. Rao, Nanoscale Res. Lett. 6 (2011) 460-467.

[6] J. Li, L. Gao, Q. Zhang, R. Feng, H. Xu, J. Wang, D. Sun, C. Xue, Journal of Nanomaterials. 2014 (2014) 1-7, Article ID 986809.

[7] W. Wu, X. H. Xiao, S.F. Zhang, Nanoscale Res. Lett. 6 (2011) 533-538.

[8] K. Vanheusden, W. L. Warren, C. H. Seager, D. R. Tallant, J. A. Voigt, and B. E. Gnade, J. Appl. Phys., 79 (1996) 7983-7990.

[9] K. Vanheusden, C. H. Seager, W. L. Warren, D. R. Tallant, and J. A. Voigt, Appl. Phys. Lett., 68 (1996) 403-405.

[10] Y. Gong, T. Andelman, G. F. Neumark, S. O'Brien, I. L. Kuskovsky, Nanoscale Res Lett 2 (2007) 297–302

[11] S. Liang, M. Li, J. H. Wang, X. L. Liu, Z. H. Hao, L. Zhou, X. F. Yu, and Q. Q. Wang, OPTICS EXPRESS. 21 (2013) 3253-3258.

[12] S. Panigrahi, and D. Basak, Chemical Physics Letters. 511 (2011) 91-96.

[13] C. Jin, H. Kim, S. Park, Y. Kwon, S. Lee, H. W. Kim and C. Lee, Advances in Applied Ceramics. 110 (2011) 270-274.

[14] S. Panigrahi, A. Bera, and D. Basak, ACS APPLIED MATERIALS & INTERFACES. 1 (2009) 2408-2411.

[15] J. D. Prades, F. H. Ramirez, R. J. Diaz, M. Manzanares, T. Andreu, A Cirera, A. R. Rodriguez, and J. R. Morante, Nanotechnology. 19 (2008) 465501-465507.

[16] Q .H. Li, T .Gao, Y. G. Wang and T. H. Wang, Appl. Phys. Lett. 86 (2006) 123117-123119

[17] Y. Lin, D. Wang, Q. Zhao, Z. Li, Y. Ma, and M. Yang, Nanotechnology. 17 (2006) 2110–2115.

[18] X. L. Fang, C. Chen, M. S. Jin, Q. Kuang, Z. X. Xie, S. Y. Xie, R. B. Huang, L. S. Zheng, J. Mater. Chem. 19 (2009) 6154−6160.

[19] Y. H. Jin, S. D. Seo, H. W. Shim, K. S. Park and D. W. Kim, Nanotechnology. 23 (2012) 125402-7.

[20] B. Sahoo, K. S. P. Devi, S. K. Sahu, S. Nayak, T. K. Maiti, D. Dhara and P. Pramanik, Biomater. Sci. 1 (2013) 647-657.

[21] F. Ahangaran, A. Hassanzadeh and S. Nouri, International Nano Letters, 3 (2013) 23-27.

[22] C. Hui, C. Shen, J. Tian, L. Bao, H. Ding, C. Li, Y. Tian, X. Shi and H. J. Gao, Nanoscale, 3 (2011) 701−705.

[23] Y. Su, G. Li, X. Bo and L. Li, Nanotechnology. 18 (2007) 485602-405607.

[24] S.K. Mishra, R.K. Srivastava, and S.G. Prakash, J. Alloys Compd. 539 (2012) 1−6.

[25] Z.-M. Liao, Z.-K. Lv, Y.-B. Zhou, J. Xu, J.-M. Zhang, and D.-P. Yu, Nanotechnology 19 (2008) 335204-335207.

[26] P. K. C. Pillai, N. Shroff, N. N. Kumar, and A. K. Tripathi, PHYSICAL REVIEW B. 32 (1985) 8228-8233.

[27] S. K. Mishra, R. K. Srivastava, S. G. Prakash, R. S. Yadav, and A. C. Pandey, Electronic Mater. Lett. 7 (2011) 31-38.

[28] Q. H. Li, T. Gao, and T. H. Wang, Appl. Phys. Lett. 86 (2005) 193109-193111.

[29] T. Gao, Q. H. Li, and T. H. Wang, Appl. Phys. Lett. 86 (2005) 173105-173107.

[30] H. Kind, H. Yan, B. Messer, M. Law, and P. Yang, Adv. Mater. 14 (2002) 158-160.

[31] Y. Muraoka, N. Takubo, and Z. Hiroi, J. Appl. Phys. 105 (2009) 103702-103708.

[32] S. H. Choi, R. G. Elliman, Appl, Phys. Lett. 74 (1999) 3987-3989.

[33] E. A. Kafadryan, S. Levichev, S. R. C. Pinto, N. R. Aghmalyanl, R. K. Hovsepyanl, G. R. Badalyan, A. Chahboun, A. G. Rolo, M. J. M. Gomes, Semicond. Sci. Technol. 23 (2008) 095025-095030.

[34] Q.H. Li, T. Gao, Y.G. Wang, T.H. Wang, Appl. Phys. Lett. 86 (2005) 123117-123119.

[35] X.G. Zheng, Q.Sh. Li, W. Hu, D. Chen, N. Zhang, M.J. Shi, J.J. Wang, L.Ch. Zhang, J. Lumin. 122 (2007) 198-201.

Figure captions:

Fig. 1: SEM morphology of (a) Fe_3O_4 (b) $Fe_3O_4@SiO_2$ (c) formation of Fe_3O_4 microsphere from large number of Fe_3O_4 nanoballs.

Fig. 2: (a)-(b) TEM images and (c) STEM-HAADF image of Fe_3O_4 microsphere. (d) TEM image and (e) STEM-HAADF image of $Fe_3O_4@SiO_2$ microsphere. (f) Selected area ('2') EDX analysis and (g) line scan EDX analysis of $Fe_3O_4@SiO_2$. (h) Elemental color mapping of $Fe_3O_4@SiO_2$ cores-shell sample.

Fig. 3: Schematic representation of formation of both Fe_3O_4 and $Fe_3O_4@SiO_2$.

Fig. 4: XRD pattern of (a) Fe_3O_4 (b) $Fe_3O_4@SiO_2$.

Fig. 5: FTIR spectra of (a) Fe_3O_4 (b) $Fe_3O_4@SiO_2$.

Fig. 6: (a) PLE measurements of both Fe_3O_4 (black line) and $Fe_3O_4@SiO_2$ (blue line) samples (b) Room temperature PL measurements of both Fe_3O_4 (black line) and $Fe_3O_4@SiO_2$ (blue line) samples at an excitation wavelength of 320 nm.

Fig. 7: Figure 6: I-V characteristics of (a) pristine Fe_3O_4 (inset image shows the device structure for the photocurrent measurement of the samples) (b) $Fe_3O_4@SiO_2$.

Fig. 8: Photocurrent rise-decay of (a) pristine Fe_3O_4 and (b) $Fe_3O_4@SiO_2$ core-shell samples respectively.

Fig. 9: Schematic representation of the mechanism of anomalous photoconductivity exhibited by $Fe_3O_4@SiO_2$.